

The bifurcation structure and noise assisted transitions in the Pleistocene glacial cycles

Peter D. Ditlevsen,

Centre for Ice and Climate, The Niels Bohr Institute,

University of Copenhagen, Juliane Maries Vej 30,

DK-2100 Copenhagen O, Denmark.

November 30, 2021

The glacial cycles are attributed to the climatic response of the orbital changes in the irradiance to the Earth (Milankovitch, 1930; Hays *et al.* , 1976). These changes in the forcing are too small to explain the observed climate variations as simple linear responses. Non-linear amplifications are necessary to account for the glacial cycles. Here an empirical model of the non-linear response is presented. From the model it is possible to assess the role of stochastic noise in comparison to the deterministic orbital forcing of the ice ages. The model is based on the bifurcation structure derived from the climate history. It indicates the dynamical origin of the Mid-Pleistocene transition (MPT) from the '41 kyr world' to the '100 kyr world'. The dominant forcing in the latter is still the 41 kyr obliquity cycle, but the bifurcation structure of the climate system is changed. The model indicates that transitions between glacial

and interglacial climate are assisted by internal stochastic noise in the period prior to the last five glacial cycles, while the last five cycles are deterministic responses to the orbital forcing.

1 Introduction

The dominant orbital periods in solar insolation is the 41 kyr obliquity cycle (tilt of rotational axis, determining the meridional gradient in insolation) and the precessional cycles (determining the season when Earth is closest to the Sun) which decompose into 19 kyr and 23 kyr periods. However, through the last 800 kyr – 1 Myr the dominant period for the glacial cycles is approximately 100 kyr similar to the one order of magnitude weaker eccentricity cycle (determining the semi-annual difference in distance to the sun). The weakness of this climatic forcing is referred to as the 100 kyr problem of the Milankovitch theory (Imbrie *et al.* , 1993). It is now generally accepted that the 100 kyr glacial time scale cannot be attributed to the eccentricity cycle (Huybers, 2007). In the Plio- and early Pleistocene, 3–1 My BP, the dominant period of variation was indeed the 41 kyr obliquity variation (Raymo *et al.* , 1989; Huybers & Wunsch, 2005).

Different mechanisms have been proposed to explain the occurrence of the 100 kyr glacial cycle. These range from self-sustained non-linear oscillators (Källen *et al.* , 1979; Saltzman & Sutera, 1987; Gildor & Tziperman, 2000), forced non-linear oscillators (LeTreut & Ghil, 1983) to stochastic or coherence resonance (Benzi *et al.* , 1982; Pelletier, 2003). Others emphasize, based on spectral analysis, the non-linear nature (Rial, 1999) and the stochastic nature of the climate signal (Kominz & Pisias, 1979; Ashkenazy *et al.* , 2005).

The non-linearity of the response to the forcing implies that a linear cross-spectral analysis between the paleoclimate record and the components of the orbital forcing does

not necessarily pick out accurately the relative weights of the different components.

Combined evidence from records of glaciations on land and deep sea records suggest that the climate has shifted between different quasi-stable states characterized by the mode of the global ocean circulation and the degree of glaciation (Imbrie *et al.* , 1992). By comparison between the paleoclimatic record and the non-linear stochastic model, it is demonstrated that the record can be generated by the forcing from insolation changes due to the obliquity cycle through the full record including the last 1 Myr. It has been long known that the '100 kyr world' is not linearly responding to the orbital forcing (Kominz & Pisias, 1979), but even in the '41 kyr world' the climate response to the orbital forcing is non-linear (Ashkenazy & Tziperman, 2004). The assumption here is that the orbital forcing resulted in periodic jumps between two stable climate states. What happened approximately 800 kyr – 1 Myr ago was that a third deep glacial state became accessible resulting in a change in length of the glacial cycles. The reason for this mid-Pleistocene transition (MPT) is unknown, and attributed to a gradual cooling due to a decreasing atmospheric CO_2 level (Saltzman & Maasch, 1991) or a change in the bedrock erosion (the regolith hypothesis) (Clark & Pollard, 1998). For a review see (Clark *et al.* , 2006).

For a simple 0-dimensional model of the Earth, where the climate is characterized by one number, the global mean temperature, there is ambiguity in ascribing the orbital forcing from the time and space varying insolation field across the globe.

In a very interesting series of papers Huybers et al. (Huybers & Wunsch, 2005; Huybers & Tziperman, 2008) argue that integrated summer insolation is the relevant measure of orbital forcing. This is closely related to the concept of degree days, which is the annual number of days with temperatures above freezing. The underlying assumption being that ablation from the glaciers is a dominant climate driver. This measure is dominated by the obliquity cycle

since, as noted by Huybers, the increased insolation when Earth is close to the sun in its orbit is compensated by shorter time spend there due to Keplers second law. Thus the total insolation during the degree days becomes independent on the precessional cycle. Here we shall assume the integrated insolation exceeding 200 W/m^2 to be a proxy for the degree days forcing.

In contrast to this Paillard (1998) shows, using a simple rule based model of jumping between three different quasi-stationary climate states, that the climate record can be a response to the summer solstice insolation at 65°N . The two proposed forcings (degree day insolation and June 26 insolation) are different, since the latter has a strong component of the precessional cycle. Using the June 26 insolation as the better proxy for the forcing can be rationalized from the point of view of a threshold crossing dynamics, since the extremal values (mid-summer insolation) would then be the governing parameter. However, since we cannot decide between the two within the framework of a simple model, we shall take the alternative approach of assuming the linear combination of the two, considered as a first order expansion, which gives the best fit between the observed record as response to the forcing.

The starting point for the model is the rule based model proposed by Paillard. The rules imposed by Palliard will be derived from an effective governing stochastic differential equation. This gives a dynamical explanation of the rule based model and potentially narrow the range of possible climate mechanisms and models capable of explaining the glacial cycles.

2 Non-linear climate response to the forcing

Due to the high dimensionality and the stochastic nature of the climate fluctuations it is highly unlikely that regular periodicities can result from internal oscillatory modes alone. It is much more plausible that non-linear responses to weak external periodic forcing would lead to periodic behaviour. There is evidence from observations as well as models that multiple states exist in the climate system (Imbrie *et al.* , 1992). This suggests a possible scenario of periodically induced destabilizations of quasi-stable climate states.

The multiple states governed by ice-albedo feedback as proposed in simple energy balance models (Sellers, 1969; Budyko, 1969) have been demonstrated in a more realistic climate model (Langen & Alexeev, 2004). Likewise it has been demonstrated that more realistic ocean models (Rahmstorf, 1995) has a structure of stability and bifurcation points similar to the simple box models (Stommel, 1961). It is thus plausible that within the high dimensional climate system there are slow manifolds for which bifurcation points exist (Broecker, 1997).

Bifurcation points in the system describe structural changes in the stability of meta-stable states as a function of a control parameter measuring the forcing of the system. The validity of linear analysis near the stable states permits a complete classification of the possible types of bifurcation points in any non-linear system (Guckenheimer & Holmes, 1986).

The paleoclimatic records, especially from deep sea cores and ice cores, show that at least three distinct climate states have been identified (Imbrie *et al.* , 1992). These are:

- (1) A deep glacial state for which the North American and Fenno-Scandian ice sheets had their full extend and the Northern Atlantic deep water formation was weakened due to the extended sea ice cover. However, more recent analysis of sediment records show that even in the deep glacial state there was a substantial thermohaline flow in the North

Atlantic (McManus *et al.* , 2004) (2) An intermediate or pre-glacial state where the ice sheets were in a slow build up phase and the Gulf Stream made way for some intermediate water formation and the boreal heat pump. (3) The interglacial state where the northern ice-sheets, except from Greenland, were gone and the deep water formation occurred as today north of Denmark straight with the Nordic heat pump. The fourth state described by Imbrie *et al.* (1992) will be regarded as a transition state here.

The three states can be identified with the ones labelled G (deep glacial), g (pre-glacial), and i (interglacial), respectively, by Paillard (1998). Here we adapt the same notation. Paillard observed in the paleoclimatic record that there seems to be "forbidden" transitions between the three states. In the period 2-1 Myr BP the record shows regular oscillations between only the two states i and g , while in the period 1-0 Myr BP there is only a specific sequence of occurrences: $i \rightarrow g \rightarrow G \rightarrow i$ permitted. The model presented here gives a dynamical explanation of this observation.

3 The stochastic model

The model, which is empirical, assumes that the climate dynamics is reflected in a single variable $x(t)$. This is as usual taken to be (minus) the global ice volume, represented by the deep sea oxygen isotope ratio, roughly proportional to global mean surface temperature anomaly. The dynamics is described by an effective non-linear stochastic differential equation,

$$dx = f_{\alpha}(x, \mu)dt + \sigma dB \tag{1}$$

where the white noise term dB with intensity σ describes the influence of the non-resolved variables and the internally generated chaotic climate fluctuations. It is within this frame-

work the roles of the orbital forcing and internal stochastic forcing is investigated. The deterministic part, $f_\alpha(x, \mu)$, of the dynamics depends on the external orbital forcing, labelled by a single control parameter μ and internal parameters, represented by α . Note that Eq. 1 is non-autonomous, since μ and α are time dependent.

The full climate dynamics can obviously not be completely reconstructed by such a single valued function. However, since stability and bifurcations are topological quantities it could be robust with respect to the detailed dynamics modelled. It is thus the bifurcation structure of $f_\alpha(x, \mu)$, with respect to the control parameter μ , which determines the climate development.

Guided by the observed record and the transition rules proposed by Paillard we can empirically construct a bifurcation diagram: Figure 1, upper panel, shows the bifurcation diagram for the drift function $f_\alpha(x, \mu)$ as a function of μ at the time interval 2 – 1 Myr BP. The bifurcation diagram shows the curves $\{x_0(\mu) | f(x_0, \mu) = 0\}$. The fat curves are the stable fixed point curves for which $\partial_x f < 0$, while the thin curves are the unstable fixed point curves for which $\partial_x f > 0$. Thus in the case of no additional noise ($\sigma = 0$ in eq. 1) the state of the system $x(t)$ is uniquely determined from the initial state $x(0)$ and the development of the forcing $\mu(t)$.

In the real climate system the internal noise is substantial and the system will not reside exactly in the steady states determined by the bifurcation diagram. Thus the full drift function needs to be parametrized. The simplest way to parametrize the drift function in accordance with the bifurcation diagram is as a fifth order polynomial:

$$f_\alpha(x, \mu) = \Pi_{j=1}^5 (x - x_\alpha^j(\mu)), \quad (2)$$

where $x_\alpha^j(\mu)$ is the j 'th steady state (zero-points) in the bifurcation diagram. As labelled

in the figure the parameter α determines the position of the lower bifurcation point. See the appendix for more details. A Matlab code of the model is available in the online supplementary material.

It should be noted that this is, of course, not the only possible drift function corresponding to this bifurcation diagram. In order to reconstruct the drift function from the observed realization, one could in principle obtain the stationary probability density $p_{\mu_0}(x)$ by sorting $x(t)$ according to $\mu(t) = \mu_0$. Assuming that $\mu(t)$ is changing slowly in comparison to the time scale for $x(t)$ to drift to a stationary state x_0 ($f_\alpha(x_0, \mu) = 0$), one could then obtain $f_\alpha(x, \mu_0)$ by solving the Fokker-Planck equation (Gardiner, 1985) associated with Eq. 1 for fixed $\mu = \mu_0$. This would require a very long data series and complete absence of additional non-climatic noise in the proxy data. This is not the case for the existing paleoclimatic record.

The climate forcing is, as mentioned before, taken to be a linear combination of the summer solstice 65N insolation (f_{ss}) and the integrated summer insolation at 65N (\bar{f}_I), where the summer period is defined as the period where the daily mean insolation exceeds $I = 200 \text{ W/m}^2$. The model results are robust with respect to the threshold I chosen in a rather broad interval. The forcing, $f = \lambda \bar{f}_I + (1 - \lambda)f_{ss}$, shown in figure 3, second panel, is calculated using the code provided by Eisenman and Huybers (Huybers & Eisenman, 2006). Values of λ around 0.5 gives the best result, $\lambda = 0.5$ is used. This assignment might, within the framework of the non-linear model, be interpreted as an empirical determination of the dominating components of the orbital forcing.

4 The hysteresis behavior

The diagram in figure 1, upper panel, shows the fixed points of $f_\alpha(x, \mu)$ as a function of the deterministic forcing μ . The three branches of stable fixed points $x^j(\mu)$ for the function, such that $f_\alpha(x^j, \mu) = 0$ and $\partial_x f_\alpha(x^j, \mu) < 0$, are indicated by fat curves. The functional form for the five functions $x^j(\mu)$ are given in the appendix. The specification of the $x^j(\mu)$'s and equations 1 and 2 completely defines the model. Since x is a proxy for global mean surface temperature anomaly (or minus global ice volume), the lower branch corresponds to the deep glacial state G . The middle branch corresponds to the climate state g and the upper branch to the interglacial state i . The thin curves correspond to the separating unstable fixed points. The dashed line-segments correspond to pairs of complex conjugate roots in the fifth order polynomial. Note again that assuming a polynomial drift function, this is uniquely determined from the roots, except from a trivial multiplicative constant.

Suppose now that the climate is in either of the states g or i and the climatic noise is too weak to induce a crossing of a barrier separating the stable states. Then the only way a forcing induced shift between the climate states can occur is through bifurcations and a hysteresis as sketched by the arrows. Clearly the climate state G is unreachable.

Assume now that the lower bifurcation point, indicated by α_0 in figure 1, upper panel, moves toward larger values of μ indicating that a stronger forcing is needed in order to destabilize the deep glacial state. In this case, $\alpha_0 \rightarrow \alpha_1$ shown in figure 1, lower panel, the glacial state G is now reachable and a hysteresis loop $i \rightarrow g \rightarrow G \rightarrow i$ will appear. The central postulate of the model is the change in this bifurcation structure represented by the shift of the point α (from α_0 to α_1 on the μ -axis) at the Mid-Pleistocene transition. This constitutes a dynamical explanation for the rule based model by Paillard (Paillard, 1998).

The change in the position of the lower bifurcation point is modelled such that $\alpha = \alpha_1$ when the climate is in state i . When the state G is reached through two bifurcations, α is gradually changing. The gradual change in the bifurcation diagram is modelled as a relaxation, $d\alpha/dt = -(\alpha - \alpha_0)/\tau$, where α_0 is the early Pleistocene equilibrium value and τ is a relaxation time. When the climate bifurcates through the rapid transition $G \rightarrow i$, the parameter α again change to α_1 .

In order for the climate to skip the 41 kyr obliquity pacing of deglaciations the timescale τ governing the bifurcation structure must be considerably longer than 41 kyr. The model results are quite insensitive to the specific value of τ in the interval 70-130 kyr, and is set to be 100 kyr. It is a major challenge to interpret the behavior of the bifurcation point α , governed by such a long time scale in terms of real climate dynamics. One could speculate that it is linked to the carbon cycle and with erosion of continents on these long time scales.

5 Comparison between the paleoclimatic record and the model

The presence of the stochastic forcing implies that the climate evolution is not fully deterministic.

Figure 2, first panel, shows a particular realization of the model. The second panel shows the forcing, the red curve shows the value of α , which is defined as the position of the lower bifurcation point in figure 1 along the axis of the forcing (the x-axis). Note that a transition $G \rightarrow i$ without noise assistance is only possible when the forcing exceeds the value of α (that is when the blue curve is above the red curve in the second panel).

The composite Atlantic ocean sedimentation record for the period 0 – 2000 kyr BP

generated by Huybers (Huybers, 2007) is shown in the bottom panel. The record is the benthic oxygen isotope sequence. The curve is plotted with normalized variance and the mean subtracted. This is a proxy for the global ice volume. The dating is based on a depth-age model independent from astronomical tuning. Note that the model resides predominantly in the deep glacial state G , rather than the pre-glacial state g . This is opposite to the model by Paillard (1998).

The differences between the single records compositing the stacked record gives an estimate of the additional noise from bioturbation and other factors that makes the record different from a true record of ice volume. So in order to compare the model with the observed climate record an additional red noise, of the same magnitude as the difference in deep sea records is added to the model. This is shown in the third panel, which should be compared with the observed record in fourth panel.

6 The role of the stochastic noise

In order to investigate the role of the stochastic noise a set of realizations of the model has are presented in figure 3. For the comparison between the model and the proxy climate records we focus on the rapid transitions $G \rightarrow i$, called terminations (Broecker, 1984; Raymo, 1997). The top panel shows a realization with no stochastic noise. This is the deterministic climate response to the orbital forcing. It is seen that the last five terminations are reproduced as observed, but there are fewer interglacials in the earlier part of the late-Pleistocene period (1000-500 kyr BP) than in the observed record. From figure 2, second panel, it is seen that the amplitude of the orbital forcing is low in this period. The bottom four panels show different realizations with a moderate stochastic forcing ($\sigma = 0.8 \text{ K}/\sqrt{\text{kyr}}$). In these realizations the added noise induces additional terminations

at different times, suggesting a fundamental unpredictability in glacial terminations.

The transitions only happens with high probabilities at times when the orbital forcing is at a local maximum and when the value of the parameter α has become low enough (see figure 2, second panel). This will typically happen every 80 kyr or every 120 kyr, which we for now will denote short (S) and long (L) iceages. A time period experiencing n short iceages and m long iceages is then denoted (nS,mL) . There are then $K(n+m,n)$ specific sequences $(S,S,L,S,L,...)$ of iceage histories with n short and m long iceages, where $K(n+m,n)=(n+m)!/(n!m!)$ is the binomial coefficient. In the last 1 Ma ice age history there is the possibility of $(11S,1L),(9S,2L),(8S,3L),(6S,4L),(5S,5L),(4S,6L),(2S,7L)$ and $(0S,8L)$. The number of possible iceage histories with only 80 kyr or 120 kyr durations is thus

$$N = K(12, 1) + K(11, 2) + K(10, 4) + K(10, 5) + K(10, 6) + K(9, 2) + K(8, 0) = 941.$$

The probabilities of transition are not equal for each maximum of the orbital forcing. It depends on two factors, the value of the parameter α , which depends on the time since the previous transition and the actual size of the forcing. However, assuming these to be equally likely, we can roughly estimate the probability for the model to reproduce exactly the observed iceage history is only around 1 permil. Note that this is a high estimate for the probability of the exact iceage history, since the possibility of 40 kyr iceages is neglected. Such an iceage occurred once in the model simulation shown in figure 2. This compares well with the observed record (figure 2, lower panel) where the marine isotope stage 7 (approx. 250 – 200 kyr BP) seems to be split into two periods.

Even though the observed iceage history is not expected to be reproduced in a given model realization, the spectral density is similar. The spectral signature of the change in the climatic record from the 41 kyr world (2–1 Myr BP) to the 100 kyr world (1–0

Myr BP) is shown in figure 4. The spectral signature is well reproduced in the randomly chosen model realization.

7 Suggestive interpretation of the dynamics

This section may be skipped without loss of continuity. The model is empirically derived from the paleoclimatic record. Since the record is only a one dimensional representation of the climate state and the high dimensional real climate variability is described as noise in an effective stochastic governing equation, the interpretation of the underlying dynamics can only be suggestive.

The climate stability can be described in terms of temperature-albedo feedbacks or equivalently ice volume-precipitation feedbacks (North *et al.* , 1981; Ghil & Childress, 1987; Tziperman & Gildor, 2003). From the latter perspective we may write the non-linear drift $f_\alpha(x, \mu) = \text{ablation (ice melt off)} - \text{accumulation (precipitation on ice sheets)}$. In figure 5 the bifurcation diagrams for the two periods are repeated (top panels) together with graphs of the accumulation and ablation curves (a-f) along the transects shown in the top panels. Going from top to bottom corresponds to increasing orbital forcing.

The ablation, $f_\alpha^{abl} = c_0 + c_1 \cdot (x - T_m)$, is assumed to be a linearly increasing function of the temperature. The constants c_0, c_1 and the effective temperature of melting T_m are related to the specific heat of melting, relation between global temperature and high latitude temperatures et cetera. It could potentially be estimated from paleo-observations of freshwater influx into the oceans. The accumulation, f_α^{acc} , is a more complex non-linear function of temperature. The accumulation is empirically determined from (2) simply as $f_\alpha^{acc} = f_\alpha - f_\alpha^{abl}$. This splitting of the drift function should be considered schematic, and attempt towards more realism would involve much more complex climate models,

which shall not be pursued here. The stable fixed points for $f_\alpha(x, \mu)$ with respect to x are marked with red circles in figure 2, panels a-f. The accumulation depends on the hydrological cycle, sea ice cover and snow to rain ratio. Furthermore, it could depend on the temperature of the deep ocean through the sea ice shift (SIS) mechanism suggested by Gildor and Tziperman (Gildor & Tziperman, 2000; Tziperman & Gildor, 2003). This is a good candidate for explaining the difference between the early Pleistocene (right panels) and the late Pleistocene (left panels) climates. The major difference is seen by comparing panels b and e in figure 2. Panel b represents the climate drift in the late Pleistocene period where the deep ocean is cold (Ruddiman *et al.*, 1989). The low temperature of the deep ocean effectively prevents heat exchange with the upper water masses, such that an extensive sea ice cover can develop (Tziperman & Gildor, 2003). The barrier separating the states G and g could be caused by a change in the hydrological cycle such that to the left of the barrier (towards state G) the accumulation decreases rapidly with temperature due to the growth of sea ice cover, while to the right of the barrier (towards state g) the accumulation decreases with increasing temperature. This could be due to the southward position of the summer polar front changing the precipitation pattern over the ice sheets. Perhaps this would result in more rainfall and less snow fall over the ice sheets as temperature increases leading to the decreasing accumulation with temperature (Tziperman & Gildor, 2003).

However, the real climate has not, except perhaps for short transient periods, been in such a state, thus it cannot be reconstructed from paleoclimatic evidence and we will have to rely on physical reasoning and future realistic climate models for explanations. In the early Pleistocene period for the same forcing the barrier is absent (panel e).

When the state i is reached, the Antarctic ice core records show that the level of atmospheric CO_2 has increased due to oceanic heating and following CO_2 release. When

the climate state G is reached after two bifurcations the atmospheric CO_2 concentration will gradually decrease as the ocean cools. Furthermore, the large glaciers build up on land.

In the late Pleistocene period when the glacial state G is reached the meridional heat transport in the oceans is strongly reduced. This would trap the warm ocean waters in the tropics, leading to a slow heating of the deep tropical ocean. This would perhaps in turn lead to an oceanic climate more similar to the one in the early Pleistocene period, where the deep ocean was warmer (Tziperman & Gildor, 2003). This could then imply the slow change of the position of the bifurcation point α in the direction of its position during the early Pleistocene period. This would make way for the orbital forcing to trigger the transition $G \rightarrow i$. The triggering of a transition is then a combination of the deterministic orbital forcing and the internal stochastic noise induced forcing.

The forcing will trigger the transition $G \rightarrow i$ way before the early Pleistocene value is reached. One could speculate that the slow heating of the tropical ocean during the state G could also be related to the lower atmospheric CO_2 concentration in the late Pleistocene period (Maasch & Saltzman, 1990; Saltzman, 1990). However, one should stress that interpretation in terms of accumulation, ablation and ocean circulation is suggestive. Only the bifurcation structure of the governing equation is obtained from the paleoclimatic records. Future realistic climate models with the same type of bifurcation structure are necessary to substantiate these speculations.

8 Summary

In summary the empirical stochastic model presented support the suggestion that the transition from the '41 kyr world' to the '100 kyr world' occurring approximately 1 Myr

- 800 kyr BP is due to a structural change in the bifurcation diagram describing the stability of the system as a function of the forcing. The glacial cycles are not solely a deterministic response to the orbital cycles. The internal noise also plays a role in triggering the jumps between the different climatic states in the first part of the '100 kyr world', this makes the ice ages fundamentally unpredictable. Currently the state-of-the-art general circulation climate models are far from being able to simulate the observed glacial climate variations. It is even not known if they possess a non-trivial bifurcation structure. This lack of dynamical range might be due to underestimation of internal variability in too coarse resolution, thus the climate noise is too weak to induce transitions from one stable climate state to another. The identification of the dynamical bifurcation diagram from observations, should be a guideline for identification of physical mechanisms and ultimately for building realistic glacial climate models.

Appendix: Parametrizing the bifurcation diagram

The fixed point curves in the hysteresis diagram determines the drift function $f_\alpha(x, \mu)$.

They are specified from parabolic curves:

$$(x^j(\mu) - f^j)^2 = (\mu - \lambda_i)^2 \Rightarrow x^j(\mu) = f^j \pm \sqrt{\mu - \lambda^j},$$

thus the bifurcation point is specified by the cartesian coordinates (λ^j, f^j) . For $\mu < \lambda$ there are two complex conjugate roots to the equation not corresponding to real fixed points. These are indicated by dashed lines in figure 1 and figure 6. For $\mu > \lambda^j$ there are two branches (a stable and an unstable) of fixed points. The branches corresponding to the intermediate glacial state 'g' and an unstable branch are thus specified as

$$x_g^\pm(\mu) = f_g \pm \sqrt{\lambda_g - \mu},$$

where the bifurcation point is $(\lambda_g, f_g) = (0.1, -3.0)$, see figure 6. Likewise there are two branches for the interglacial state:

$$x_i^\pm(\mu) = f_i \pm \sqrt{\lambda_i - \mu},$$

with $(\lambda_i, f_i) = (-0.3, -0.5)$ and for the deep glacial state:

$$x_G^\pm(\mu) = f_G \pm \sqrt{\lambda_G - \mu},$$

with $(\lambda_G, f_G) = (\alpha(t), -4.0)$. The parameter $\alpha(t)$ thus determines the horizontal position of the lower bifurcation point in figure 6. Now, as seen in figure 6, only the upper (stable) branch, x_i^+ , and the lower (stable) branch, x_G^- , are plotted. The curve connecting the two bifurcation points is simply given as a linear interpolation between the two unstable branches:

$$x_{iG} = (1 - \lambda)x_i^- + \lambda x_G^+,$$

where $\lambda = (\mu - \lambda_G)/(\lambda_i - \lambda_G)$ and $\lambda_i \leq \mu \leq \lambda_G$. By this the five fixed points are now defined and the drift function is

$$f_\alpha(x, \mu) = -(x - x_g^+)(x - x_g^-)(x - x_i^+)(x - x_G^-)(x - x_{iG}).$$

The first minus sign ensures that $f > 0$ for $x \rightarrow -\infty$ and $f < 0$ for $x \rightarrow \infty$ as it should. This is the form specified in equation 2. The parameter $\alpha(t)$ is specified from the climate state. If the climate is in the interglacial state the parameter is set to $\alpha = \alpha_1$. When the climate jumps to the glacial state 'G', the parameter change by an exponential decay to α_0 with timescale τ :

$$\frac{d(\alpha - \alpha_0)}{dt} = -\frac{(\alpha - \alpha_0)}{\tau}.$$

The parameters used here are $(\tau, \alpha_0, \alpha_1) = (10^5 yr, 0.5, 2.2)$.

Acknowledgement: This research was supported in part by the National Science Foundation under Grant No. PHY05-51164.

References

- Ashkenazy, Y., & Tziperman, E. 2004. Are the 41 kyr oscillations a linear response to Milankovitch forcing? *Quaternary Science Reviews*, **23**, 1879–1890.
- Ashkenazy, Y., Baker, D. R., & Gildor, H. 2005. Simple stochastic models for glacial dynamics. *J. Geophys. Res.*, **110**, C022005.
- Benzi, R., Parisi, G., Sutera, A., & Vulpiani, A. 1982. Stochastic resonance in climate change. *Tellus*, **34**, 10–16.
- Broecker, S. W. 1984. Terminations. *Pages 687–698 of: Berger, A., Imbrie, J., Hays, J., Kukla, G., & Saltzman, B. (eds), Milankovitch and Climate: Understanding the Response to Astronomical Forcing.*
- Broecker, W. S. 1997. Thermohaline Circulation, the Achilles Heel of Our Climate System: Will Man-Made CO₂ Upset the Current Balance? *Science*, **278**, 1582–1588.
- Budyko, M. I. 1969. The effect of solar radiation variations on the climate of the Earth. *Tellus*, **21**, 611–619.
- Clark, P. U., & Pollard, D. 1998. Origin of the Middle Pleistocene Transition by Ice Sheet Erosion of Regolith. *Paleoceanography*, **13**, 1–9.
- Clark, P. U., Archer, D., Pollard, D., Blum, J. D., Rial, J. A., Brovkin, V., Mix, A. C., Pisias, N. G., & Roy, M. 2006. The middle Pleistocene transition: characteristics, mechanisms, and implication for long-term changes in atmospheric pCO₂. *Quaternary Science Reviews*, **25**, 3150–3184.
- Gardiner, C.W. 1985. *Handbook of Stochastic Methods*. Springer Verlag, N.Y.

- Ghil, M., & Childress, S. 1987. *Topics in Geophysical Fluid Dynamics: Atmospheric Dynamics, Dynamo Theory, and Climate Dynamics*. Springer Verlag, N. Y.
- Gildor, H., & Tziperman, E. 2000. Sea ice as the glacial cycles' climate switch: Role of seasonal and orbital forcing. *Paleoceanography*, **15**, 605–615.
- Guckenheimer, J., & Holmes, P. 1986. *Nonlinear Oscillations, Dynamical Systems, and Bifurcations of Vector Fields*. Springer-Verlag, New York.
- Hays, J., Imbrie, J., & Shackleton, N. 1976. Variations in earth's orbit: Pacemaker of the ice ages. *Science*, **194**, 1121–1132.
- Huybers, P. 2007. Glacial variability over the last 2Ma: an extended depth-derived age-model, continuous obliquity pacing, and the Pleistocene progression. *Quaternary Science Reviews*, **26**, 37–55.
- Huybers, P., & Eisenman, I. 2006. Integrated summer insolation calculations. *NOAA/NCDC Paleoclimatology Program*, **Data Contribution # 2006-079**, <http://www.ncdc.noaa.gov/paleo/forcing.html>.
- Huybers, P., & Tziperman, E. 2008. Integrated summer insolation forcing and 40,000 year glacial cycles: the perspective from an icesheet/energy-balance model. *Paleoceanography*, **23**, PAI208.
- Huybers, P., & Wunsch, C. 2005. Obliquity pacing of the late Pleistocene glacial terminations. *Nature*, **434**, 491–494.
- Imbrie, J., *et al.* . 1992. On the structure and origin of major glacial cycles. 1. Linear responses to Milankovitch Forcing. *Paleoceanography*, **7**, 701–738.

- Imbrie, J., *et al.* . 1993. On the structure and origin of major glacial cycles. 2. The 100,000-year cycle. *Paleoceanography*, **8**, 699–735.
- Källen, E., Crafoord, C., & Ghil, M. 1979. Free oscillations in a climate model with ice-sheet dynamics. *J. Atmos. Sci.*, **36**, 2292–2303.
- Kominz, M. A., & Pisias, N. G. 1979. Pleistocene Climate: Deterministic or Stochastic. *Science*, **204**, 171–172.
- Langen, P. L., & Alexeev, V. A. 2004. Multiple equilibria and asymmetric climates in the CCM3 coupled to an oceanic mixed layer with thermodynamic sea ice. *Geophys. Res. Lett.*, **31**, L04201.
- LeTreut, H., & Ghil, M. 1983. Orbital forcing, climate interactions, and glacial cycles. *J. Geophys. Res.*, **88**, 5167–5190.
- Maasch, K., & Saltzman, B. 1990. A low-order dynamical model of global climate variability over the full Pleistocene. *J. Geophys. Res.*, **95**, 1955–1963.
- McManus, J. F., Francois, R., Gherardi, J.-M., Keigwin, L. D., & Brown-Leger, S. 2004. Collapse and rapid resumption of Atlantic meridional circulation linked to deglacial climate changes. *Nature*, **428**, 834–837.
- Milankovitch, M. 1930. *Mathematische Klimalehre und Astronomische Theorie der Klimaschwankungen, Handbuch der Klimalogie Band 1 Teil A*. Borntrager Berlin.
- North, G., Cahalan, R., & Moeng, R. 1981. Energy balance climate models. *Rev. Geophys. Space Phys.*, **19**, 90–121.
- Paillard, D. 1998. The timing of Pleistocene glaciations from a simple multiple-state climate model. *Nature*, **391**, 378–381.

- Pelletier, J. D. 2003. Coherence resonance and ice ages. *J. Geophys. Res.*, **108(D20)**, 4645, doi:10.1029/2002JD003120.
- Rahmstorf, S. 1995. Bifurcations of the Atlantic thermohaline circulation in response to changes in the hydrological cycle. *Nature*, **378**, 145–149.
- Raymo, M. E. 1997. The timing of major climate terminations. *Paleoceanography*, **12**, 577–585.
- Raymo, M. E., Ruddiman, W. F., Backman, J., Clement, B. M., & Martinson, D. G. 1989. Late Pleiocene variations in Northern hemisphere ice sheets and North atlantic deep water circulation. *Paleoceanography*, **4**, 413–446.
- Rial, J. A. 1999. Pacemaking the Ice Ages by Frequency Modulation of Earth's Orbital Eccentricity. *Science*, **285**, 564–568.
- Ruddiman, W., Raymo, M., Martinson, D., Clement, B., & Blackman, J. 1989. Pleistocene evolution: Northern hemisphere ice sheets and North Atlantic ocean. *Paleoceanography*, **4**, 353–412.
- Saltzman, B. 1990. Three basic problems of paleoclimatic modeling: a personal perspective and review. *Clim. Dyn.*, **5**, 67–78.
- Saltzman, B., & Maasch, K. A. 1991. A first-order global model of late Cenozoic climatic change. *Climate Dynamics*, **5**, 201–210.
- Saltzman, B., & Sutera, A. 1987. The Mid-Quaternary Climate Transition as the Free Response of a Three-Variable Dynamical Model. *Journ. Atmos. Sci.*, **44**, 236–241.
- Sellers, W. D. 1969. A Global Climatic Model Based on the Energy Balance of the Earth-Atmosphere System. *Journ. Applied Meteorology*, **8**, 392–400.

Stommel, H. 1961. Thermohaline convection with two stable regimes of flow. *Tellus*, **13**, 224–230.

Tziperman, E., & Gildor, H. 2003. On the mid-Pleistocene transition to 100-kyr glacial cycles and the asymmetry between glaciation and deglaciation times. *Paleoceanography*, **18**, 1–8.

FIGURE CAPTIONS

Fig. 1 The bifurcation diagram for the model. Along the x-axis is the forcing represented by the control parameter μ , along the y-axis are the fixed points $\{x_0(\mu) | f(x_0, \mu) = 0\}$ of the drift function $f_\alpha(x, \mu)$. The drift function is simply approximated by a fifth order polynomial, with the roots determined by the fixed points. The horizontal dashed line-segments indicates (real part of) sets of complex conjugate roots. The fat curves show the stable fixed points. The bifurcation point α is the point where the deep glacial state G disappears. The arrows indicate the hysteresis loop as the forcing parameter is changed. Upper panel: The glacial state G is not accessible. Lower panel: Now the location of the bifurcation point α has changed in such a way that the deep glacial state G is accessible.

Fig. 2 The top panel shows a realization of the model. Second panel shows the orbital forcing driving the model. The red curve shows $\alpha(t)$, where the jumps to $\alpha = \alpha_1$ are triggered by the transition $G \rightarrow i$. The next transition is in the low noise limit only possible when the blue curve is above the red curve. The third panel shows a "pseudo paleorecord", where a red noise component representing the non-climatic noise, is added to the model realization in the top panel. Lower panel shows the (normalized) paleoclimatic isotope record from a composite of ocean cores. The record is a proxy for the global sea level or minus the global ice volume. See text for more explanations.

Fig. 3 Five realizations of the model with the same orbital forcing and different stochastic forcing. The first panel shows a realization without stochastic forcing. This is the purely deterministic climate response to the orbital forcing. The bottom four realizations has a noise intensity $\sigma = 0.8 \text{ K}/\sqrt{\text{kyr}}$. It is seen that only in the last

part of the 100 kyr world the timing of the terminations are independent from the noise. In all five realizations an additional non-climatic "proxy noise" is added aposteriori.

Fig. 4 Upper panel: The spectral power of the sediment records for the two periods, 0-1 Myr and 1-2 Myr. The red markers indicate 100 kyr, 41 kyr and 23 kyr periods. The lower panels show the corresponding spectra for the randomly chosen realization of the model shown in figure 3. Both the climate record and the model show a transition from the '41 kyr world' to the '100 kyr world'.

Fig. 5 The form of the drift function as a function of the orbital forcing. The panels a-c corresponds to the vertical intersections in the top left panel. The panels d-f are the intersections in the top right panel. The major difference between the late Pleistocene and early Pleistocene periods is seen by comparing panels b and e corresponding to the same orbital forcing in the two periods. When the climate is in the glacial state G , there will be a slow lowering of the barrier separating G and g indicated by arrows in top left panel and panel b. The (arbitrary) splitting of the drift function into an ablation part and an accumulation part is only suggestive.

Fig. 6 The bifurcation diagram with stable branches x_i^+ , x_g^+ and x_G^- . The three bifurcation points are $(\mu, x(\mu)) = (\lambda_i, f_i)$ where the interglacial state disappears, (λ_g, f_g) where the intermediate glacial state disappears and finally (λ_G, f_G) where the deep glacial state disappears. See text for explanation.

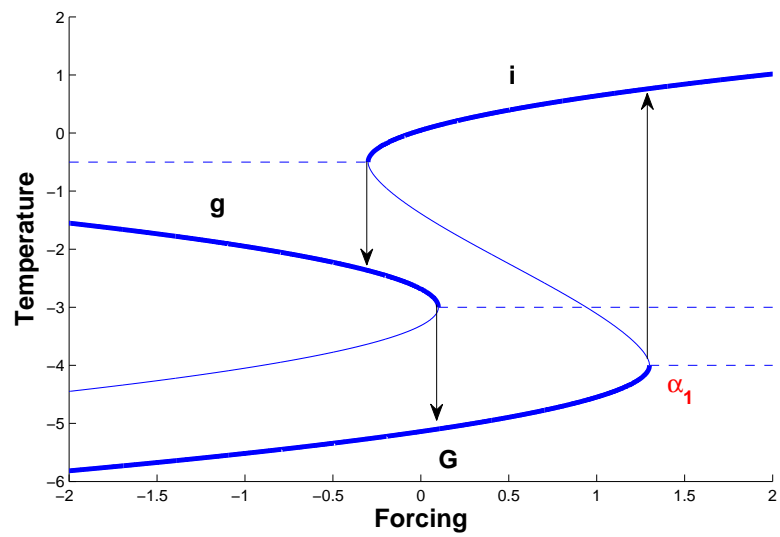
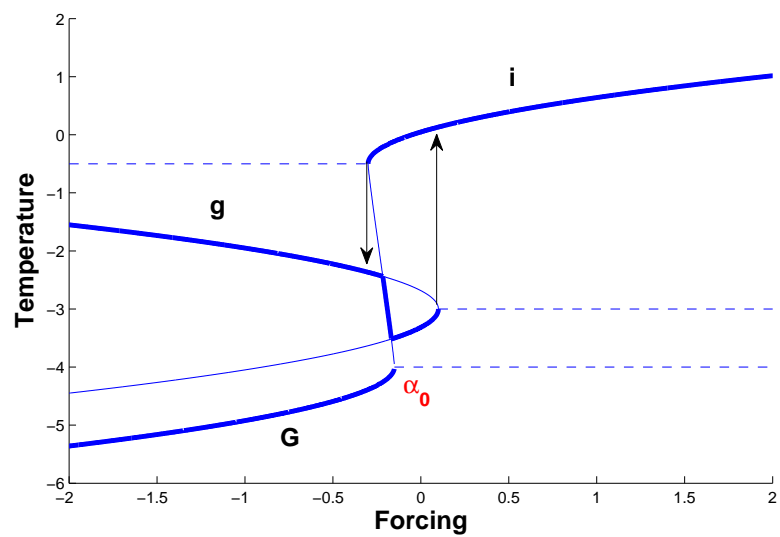


Figure 1:

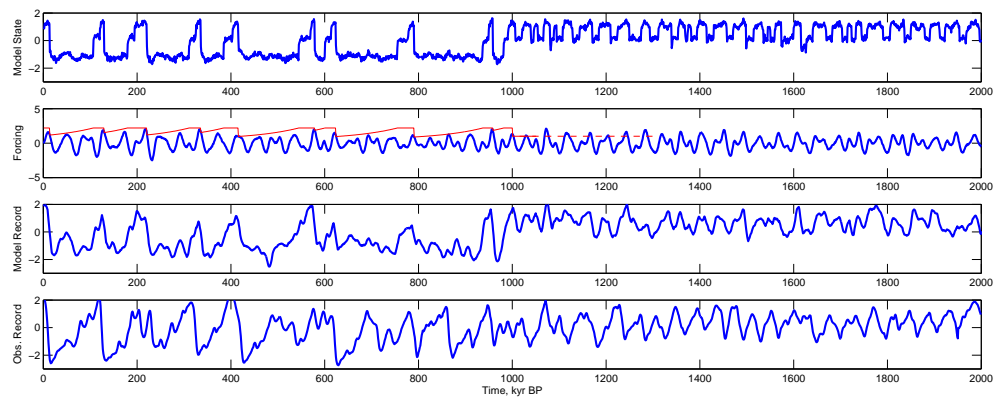


Figure 2:

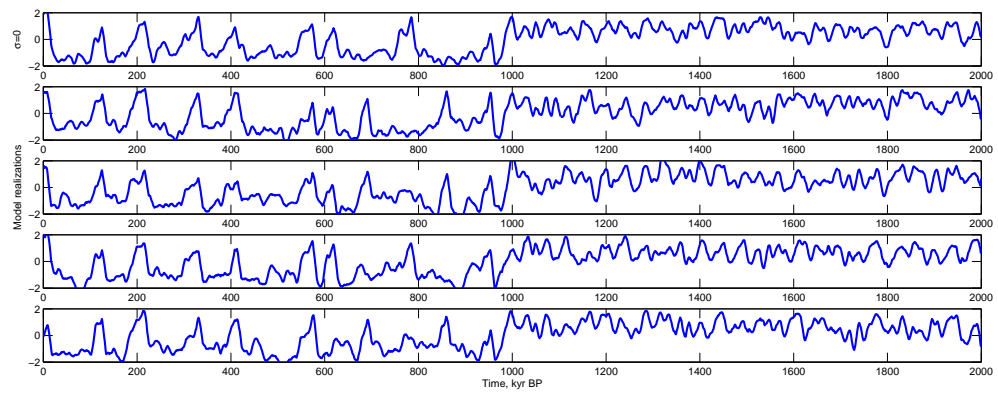


Figure 3:

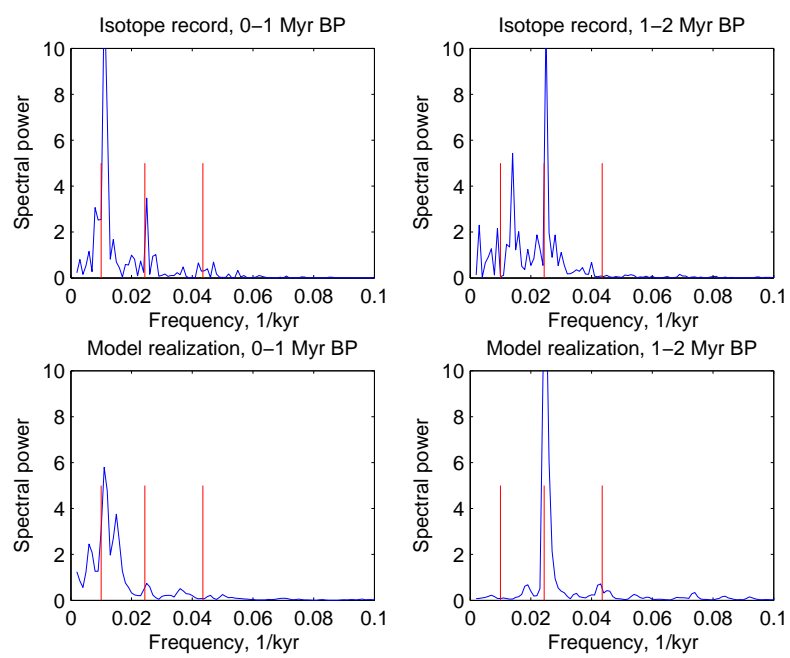


Figure 4:

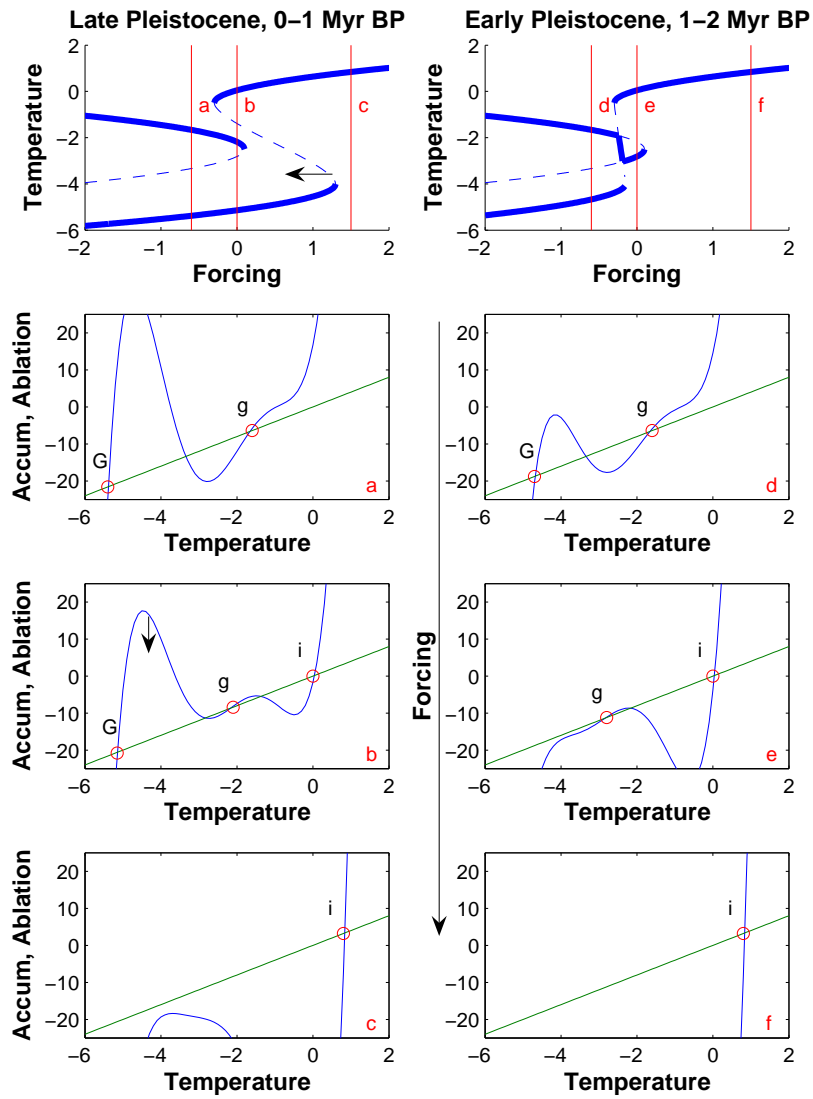


Figure 5:

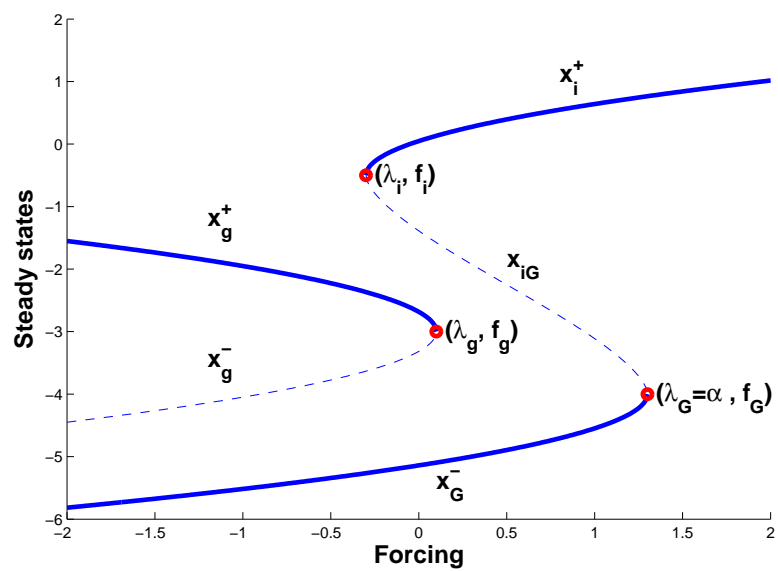


Figure 6: